Journal of Power Sources 238 (2013) 376–387

Contents lists available at SciVerse ScienceDirect

Journal of Power Sources

journal homepage: www.elsevier.com/locate/jpowsour

Review

Metal oxide hollow nanostructures: Fabrication and Li storage performance

Wei Wei [a], Zonghua Wang [b], Zhuang Liu [c], Yang Liu [c], Liang He [a], Dezhi Chen [a], Ahmad Umar [d,e,**], Lin Guo [a,*], Jinghong Li [c,*]

[a] School of Chemistry and Environment, Beihang University, Beijing 100191, China
[b] College of Chemical and Environment Engineering, Qingdao University, Qingdao 266071, China
[c] Department of Chemistry, Tsinghua University, Beijing 100084, China
[d] Department of Chemistry, Faculty of Arts and Sciences, Najran University, Najran 11001, Saudi Arabia
[e] Promising Centre for Sensors and Electronic Devices (PCSED), Najran University, Najran 11001, Saudi Arabia

HIGHLIGHTS

- Reviewed the commonly synthetic methods to create metal oxide hollow nanostructures.
- Comment on the advantages and shortages of each method.
- Shows the excellent Li storage property of metal oxide hollow nanostructures.
- Discussed the challenge and future of metal oxide hollow nanostructures anodes.

ARTICLE INFO

Article history:
Received 8 November 2012
Received in revised form
27 March 2013
Accepted 29 March 2013
Available online 7 May 2013

Keywords:
Metal oxides
Hollow nanostructure
Anode material
Li ion battery

ABSTRACT

Metal oxides, such as SnO_2, Fe_2O_3, CoO, Co_3O_4, NiO, CuO and MnO_2 etc., are promising anode materials for lithium-ion batteries due to their high capacity and safety characteristics. However, the commercial utility of metal oxide anodes has been hindered to date by their poor cycling performance. Recent study shows that metal oxides with hollow nano/microstructures exhibit fascinating performance as anode materials for Li ion batteries. In this review, we first describe the current commonly used synthetic methods to create metal oxide hollow structures, and for each method, we also comment on its advantages and shortages compared with other methods. According to some typical examples and the following theoretical analysis, we show the promising use of hollow metal oxides as anode materials for lithium-ion batteries. Finally, the challenges and future developments of metal oxide hollow structures are further discussed.

1. Introduction

By the 21st century, concerns about the shortage of fossil fuels and the needs to decrease greenhouse gas emissions, coupled with the deterioration of environment, have brought people to consider the renewable energy in large scale. Meanwhile, the efficient energy storage system is highly required. Since the early 1990's, due to their high capacity, long cycle life, low self-discharge rate and absence of "memory effect", rechargeable lithium-ion batteries (LIBs) have proved themselves as one of the most advanced chemical energy storage devices and hence recently almost dominate the portable electronics market. However, more efforts are still needed to upgrade the performances of LIBs for their further applications in various large electrical appliances such as electric vehicles (EVs) and hybrid electric vehicles (HEVs) as these devices require high capacity, power density and especially safety. Electrode materials are determined factor for the performance of the LIBs. Currently, graphite is used as an efficient anode material for LIBs because of its long cycle life, abundant material supply and relatively low cost. Even though widely used, the graphite, as an anode material, has several disadvantages such as low energy density (372 mAh g^{-1}), safety problems and so on [1,2]. Therefore, there is a great need to search and develop alternative anode materials with enhanced safety and energy density.

In the past two decades, metal oxides including transition-metal oxides (M_xO_y, M = Fe, Co, Ni, Mn, Cu, etc.) and some main group metal oxides (e.g. SnO_2, etc.) have shown their significantly higher

* Corresponding authors. Tel./fax: +86 10 62795290.
** Corresponding author. Department of Chemistry, Faculty of Arts and Sciences, Najran University, Najran 11001, Saudi Arabia.
E-mail address: jhli@mail.tsinghua.edu.cn (J. Li).

0378-7753/$ – see front matter
http://dx.doi.org/10.1016/j.jpowsour.2013.03.173

capacities and better safety characteristics than those of graphite anodes [3–13]. In this work, we first begin with a brief review of the metal oxides anodes, pointing out the advantages and disadvantages of metal oxides as LIBs anode materials and listing the common methods used to modify their electrochemical performance. Our work focuses on the hollow nanostructured metal oxides, because they not only bring us the advantages similar to other nanomaterials, but also exhibit the unique advantages – their hollow cavities can effectively improve the electrochemical performance. Herein, we point out that, the hollow nanostructures mentioned in this review mainly include hollow spheres, multi-shelled hollow spheres, core/shell structure, nanotubes, nanoboxes, etc. The synthesis methods and Li storage performances of some familiar metal oxide hollow nanostructures, such as SnO_2, Fe_2O_3, CoO, Co_3O_4, NiO, CuO and MnO_2, etc., will be discussed in separate sections. Finally, different aspects of hollow metal oxide nanomaterials, reported in the literature, i.e. from preparation to their effective utilization as anode materials for LIBs will be concluded and the future prospects of these nanomaterials will be discussed.

2. Metal oxide anode materials

2.1. Classification and Li storage mechanism

Based on the differences between Li storage mechanisms, metal oxides anodes can be divided into three groups, alloy model, displacement model and intercalation model. The description of each group is mentioned below:

2.1.1. Alloy model

Alloy model is based on the reversible charging-discharging in metal oxides. It includes two key processes, i.e. metal alloying and de-alloying. In the first process, the metal oxide is irreversibly converted or reduced to metal that is subsequently dispersed in the matrix of lithium oxide. In the next step, the metal reacts with lithium ions to form a variety of Li–M alloys during the charging process, and the reversible de-alloying of the Li–M alloys occurs in the following discharging process. It is just these alloying/de-alloying processes that give the metal oxide Li storage capacity. The overall reaction process for alloy model can be described by the below equations:

$$2x\mathrm{Li}^+ + 2xe^- + \mathrm{MO}_x \rightarrow x\mathrm{Li_2O} + \mathrm{M} \tag{1}$$

$$y\mathrm{Li}^+ + ye^- + \mathrm{M} \leftrightarrow \mathrm{Li}_y\mathrm{M} \tag{2}$$

Several metal oxides such as Ge-, Sn-, Sb-, In- and Pb-based oxides follow the alloy model process [3].

2.1.2. Displacement model

In the displacement model, the mechanism involves the reversible formation and decomposition of Li_2O, accompanying the reduction and oxidation of transition metal nanoparticles in the range of 1–10 nm. The electrochemically driven nanosized confinement of the metal particles is believed to enhance their electrochemical reactivity. The electrochemical reaction mechanism for displacement model can be written as follows:

$$\mathrm{MO}_x + 2x\mathrm{Li} \leftrightarrow x\mathrm{Li_2O} + \mathrm{M} \tag{3}$$

M is a transition metal such as Cr, Mn, Fe, Co, Ni, or Cu etc. [4].

2.1.3. Intercalation model

For metal oxides with layered structures, Li-ion intercalation/deintercalation can occur in the open channels of layered structures through diffusion, while the structural integrity of the host lattice is normally conserved. The intercalation/deintercalation reactions typically occur around room temperature. The electrochemical reaction mechanism for intercalation model can be written as follows:

$$\mathrm{MO}_x + y\mathrm{Li}^+ + ye^- \leftrightarrow \mathrm{Li}_y\mathrm{MO}_x \tag{4}$$

Several metal oxides such as MoO_2, MoO_3, WO_3 and TiO_2 etc., are examples that follow the intercalation model process [3].

2.2. Advantages and limitations of metal oxides as anode materials for LIBs

There are several key requirements necessary for an anode material in rechargeable LIBs. The requirements are as follows:

(1) The anode material should react with lithium in a reversible manner and the voltage should be low.
(2) The anode material should exhibit high capacity.
(3) The anode material should possess good electronic conductivity.
(4) The anode material should exhibit good structural stability which in fact leads to the long cycle life.
(5) The material should be chemically and biologically safe.

Based on the above requirements for good anode materials, the advantages and disadvantages of metal oxides as anode materials for LIBs have been mentioned with reference to the currently used graphite anodes. Compared with the graphite anodes, the obvious advantages of the metal oxide anodes are their high capacity and safety characteristics. Table 1 shows the theoretical capacities of some metal oxide anode materials.

Currently, the practical use of metal oxides in LIBs is mainly hampered by their intrinsic low charge/ionic conductivity and poor long-term cycling stability, which indicates that they cannot well meet with the requirements mentioned in (3) and (4). For the metal oxides that follow the Li alloy model, such as SnO_2, the practical utilization of them in secondary batteries is hindered due to the dramatic volume change associated with the alloying and de-alloying process. For SnO_2, the reaction of SnO_2 with Li excessively increases the volume which leads to abruption between the yield nanoparticles and the current collector, and hence the disintegration of the electrodes, resulting in poor cycling performance. Similar to the Li-alloying process, metal oxide anodes that follow the conversion reaction of the displacement or intercalation models also yield large volume variation upon the electrochemical cycling. Additionally, the poor electronic conductivity of the metal oxides leads to the polarization of the electrode even at a very low current rate, thus greatly decreases the power density of LIBs.

Table 1
Theoretical capacities of some familiar metal oxide anode materials.

Metal oxides	Specific capacity (mAh g^{-1})	Literature and explanations
Cr_2O_3	1058	[6]
MnO	755	[7]
MnO_2	1233	[6]
SnO_2	782	[8]
SnO	875	4.4 mol Li per mol Sn
Fe_2O_3	1007	[9]
Fe_3O_4	926	[10]
CoO	715	[11]
Co_3O_4	890	[12]
NiO	718	[6]
CuO	674	[13]
MoO_2	1117	[6]

2.3. Strategy of hollow nanostructures

To overcome the problems related with metal oxide anodes for LIBs, several strategies have been developed during the past decades and reported in the literature [14–26]. These strategies can be divided into several categories as follows: (I) The first strategy is to prepare composite electrodes with other efficient materials, such as carbon [14], carbon nanotubes [15], graphene [16–18], conductive polymers [19], and so on. These conductive matrixes used to prepare composite electrodes, not only act as physical buffering layer for the large volume changes but also as conductor which could enhance the electronic conductivity of the electrode. (II) Another strategy is to prepare various nanomaterials-based electrodes. Various morphologies of nanomaterials, such as hollow structures [12,20], mesoporous structures [21,22], nanowire arrays [23,24] and thin films [25,26] etc., can be used for this purpose.

The utilization of nanostructured materials opens up a new and important avenue in the advancement of the science and technology of LIBs applications. There are several advantages of the use of nanomaterials as electrodes for LIBs over bulk materials: higher electrode/electrolyte contact area, short path lengths for Li^+ transport, high power performance and new reactions, which are not possible with bulk materials. Compared with the other morphologies of nanostructured metal oxides, the hollow metal oxide nanostructures exhibit special characteristics and advantages as anode material for LIBs.

The advantages of metal oxide hollow nanostructures as anode materials for LIBs can be summarized as follows: Firstly, the local empty space could partially accommodate the large volume change during cycling, thus delaying capacity fading. Secondly, the hollow structures possess higher surface area, and particularly, the cavities in hollow structures may provide extra space for the storage of lithium ions which is highly beneficial for enhancing specific capacity. Thirdly, lithium could go through a surface path, facilitating lithium diffusion and allowing better reaction kinetics at the electrode surface. Moreover, hollow nanostructures could exhibit excellent C-rate performances. Due to the excellent properties and wide applications of hollow nanostructures, there are several methods that have been developed to synthesize these kinds of nanostructures and reported in the literature [10,12,20,27–74].

In the following sections, overview on the synthesis techniques and electrochemical performances of various metal oxide hollow nanostructures will be presented.

3. Synthesis methods of hollow metal oxide nanomaterials

There are two distinct strategies that are widely used for the preparation of metal oxides hollow nanostructures, i.e. template-based fabrication method and template-free fabrication method. The details of each method are described below.

3.1. Template fabrication method

Template method is probably the most effective and general method for the preparation of hollow metal oxide nanomaterials. The basis of the template-directed synthesis is the adsorption of nanoparticles on various removable templates. Based on the materials, the template fabrication method is divided into two main categories: hard template directed synthesis and soft template directed synthesis methods.

3.1.1. Hard template directed synthesis method

For the hard template method, generally "rigid materials" are used as templates. The examples of hard templates are mono-dispersed silica spheres, carbon, polystyrene (PS) spheres, metal oxides, metal salts and so on. Due to the wide existence of the target hard templates, many metal oxides hollow nanostructures can be obtained by hard template method. To clearly understand the hard template directed synthesis method to prepare hollow nanomaterials, a few examples are described:

(I) Mono-dispersed silica templates. Silica is a promising, appropriate matrix for making hollow nanostructures since this material has a low cytotoxicity, high surface area, large pore volume, and tunable pore size. The general procedure involves the casting of silica templates by suitable inorganic precursors and the removal of the silica templates by etching using NaOH or HF. For example, using the mesoporous silica "nanoreactors", Ding et al. prepared SnO_2 hollow spheres with uniform size distribution and good structural stability [28]. For the fabrication of SnO_2 hollow spheres, firstly, the concentrated $SnCl_2$ salt solution was allowed to diffuse into the hollow cavity of the SiO_2 nanoreactors via the mesoporous shell. After the thermal treatment, the $SnCl_2$ precursor was transformed to SnO_2 *in situ* and led to the formation of double-shell SnO_2@SiO_2 hollow structure. At last, the outer SiO_2 shell was removed by HF etching and finally SnO_2 hollow spheres were obtained.

In another report, Lou et al. reported the synthesis of double-walled SnO_2 "nanococoons" by facile deposition of polycrystalline SnO_2 on oval-shaped silica-based templates derived from hematite nanospindles [29]. Crowley et al. have demonstrated that Fe, Co, Ni metals and metal oxides hollow structures can be synthesized within the silica mesopores by controlling the precursor's concentration [30].

(II) Metal oxide templates. The anodized aluminum oxide (AAO) is one of the most commonly used templates to prepare metal oxide nanotubes. AAO exhibits regular porous channels and it can be fabricated by electrochemical oxidation of aluminum in acidic solutions. By controlling and changing the electrochemical oxidation parameters such as temperature, concentration, current density, and other parameters of the anodization process, the pore and diameter of the AAO templates can be adjusted. AAO templates are commonly used to synthesize metal oxide hollow structures because of the following several advantages. Firstly, they have uniform pores of high density and are chemically stable at least 700 °C. Secondly, they can be easily removed by well-established methods. In addition, the most important thing is that these AAO templates are commercially available. There are several reports which exhibit the utilization of AAO as template for the fabrication of hollow nanomaterials. Wang et al. reported an AAO templating method to prepare SnO_2 nanotubes [31]. The synthetic approach involves an infiltration casting of premade colloidal SnO_2 nanoparticles into 1-D channels of AAO membranes, the generation of chemical binding among nanoparticles via thermal treatment, and the removal of AAO templates in NaOH solutions. The as-prepared SnO_2 nanotubes were mesoporous with very uniform morphology and constant diameters in the range of 180–230 nm. Moreover, by utilizing AAO templates, free-standing CuO nanotube arrays have been prepared by using a chemical vapor deposition (CVD) method [32]. Reddy et al. have prepared coaxial MnO_2/carbon nanotube arrays using AAO templates [33]. The coaxial nanotube structures were prepared by a combination of simple vacuum infiltration and CVD techniques through a template approach. MnO_2 nanotubes were first fabricated by vacuum infiltration inside the channels of commercially available AAO templates, which was followed by the growth of

CNTs using CVD method. After removing the alumina templates with NaOH solution, the MnO_2/CNT hybrid coaxial structures were obtained.

Recently, Cu_2O appeared as a novel metal oxide template to prepare other metal oxide hollow nanostructures. The Cu_2O templates have several advantages: i) there are various morphologies of Cu_2O, such as sphere, cube, octahedra, and other highly symmetrical structures and hence utilizing such diverse morphological templates, the morphologies of hollow nanomaterials can be controlled, ii) the Cu_2O are chemically reactive, iii) the Cu_2O templates can easily be removed by acid or alkali. By applying Cu_2O as a template, recently, Lou's group prepared SnO_2 nanoboxes with controllable particle size based on the Cu_2O templates and reported in the literature [34]. As shown in Fig. 1A, in the initial step, $SnCl_4$ reacts with Cu_2O and results in a SnO_2 layer and insoluble CuCl. The CuCl was immediately dissolved by coordinating with Cl^- to form soluble $[CuCl_x]^{1-x}$. SnO_2 nanoboxes were formed when the Cu_2O template was completely consumed. Fig. 1B shows the TEM image of SnO_2 nanoboxes. The same group also prepared $Cu_2O@Fe_2O_3$ and $Cu@Fe_3O_4$ rattles, Fe_2O_3 and Fe_3O_4 cages, double shelled cages, MnO_x and Au hollow structures based on the similar mechanisms as mentioned in the case of SnO_2 nanoboxes [35]. In addition, the Cu_2O templates can also be used to prepare other hollow structures [36,37].

(III) Carbon based materials. Carbon materials including carbon spheres, fibers and nanotubes are usually employed to prepare metal oxide hollow nanostructures. Carbonaceous spheres and fibers are porous and hydrophilic, so that the inorganic metal oxide precursor solution can readily mix with the template. Metal oxide hollow structures are generated when the templates are removed by combustion. As there are many functional groups existing on the surfaces of the carbon templates, no surface modification or activation steps are required. So, this greatly reduced the processing steps and thus consumed less time compared with other templates. For example, mesoporous spheres of metal oxides were synthesized by using mesoporous carbon [38]. Hollow metal oxide nanofibers with a hierarchical architecture were synthesized by using activated carbon fibers as templates [39]. Bang et al. reported a sonochemical fabrication of crystalline hollow hematite (α-Fe_2O_3) using carbon nanoparticles as a spontaneously removable template [40]. By using carbon spheres, Jagadeesan et al. synthesized single crystalline α-Fe_2O_3 nanospheres and nanocups [41]. The morphology can be easily controlled by simply adjusting the calcination temperature. In another report, Xu and co-workers have reported the synthesis of uniform hollow nanospheres of NiO, α-Fe_2O_3, ZnO, CuO and Ga_2O_3 using carbonaceous polysaccharide nanospheres as hard templates by controlling precipitation method [42]. Even though carbon materials are effectively used to prepare hollow nanomaterials, however, challenges still exist because the hollow structure often collapses during the removal of the templates. Zhang et al. were able to overcome this problem by a dual template method [43]. The dual template consists of a MWCNTs core and a carbonaceous coating layer. Metal oxide nanotubes including SnO_2 and Fe_2O_3 were fabricated using this template method and stable nanostructures were found, which perfectly duplicated the precursor's morphology. The synthetic process can be briefly described as follows: during the hydrothermal treatment, carbonaceous layer was coated on the carbon nanotube to form dual templates. Then the metal salts were loaded on the carbonaceous layer. By calcinating the sample at a relatively low temperature (280 or 400 °C) in air, the metal salts were converted into metal oxides. At the same time, the carbonaceous layer was removed while the MWCNT remained intact, thus MWCNTs@MO composites were obtained. When the calcination temperature was elevated to 550 °C, MWCNTs were combusted, leaving metal oxide nanotubes or hollow nanomaterials only.

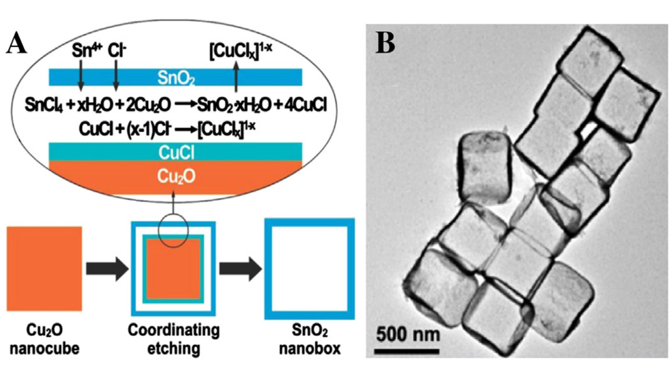

Fig. 1. A) Schematic illustration of the formation of SnO_2 nanoboxes and B) TEM image of SnO_2 nanoboxes. Reproduced from [34]. Copyright 2011, American Chemical Society.

In some reactions, carbon spheres not only act as a "rigid" template to form the metal oxide hollow structures, but also participate in the reaction process. Wang et al. described a carbon-based reactive template method to synthesize MnO_2 hollow spheres without the heat treatment [44], which is typically needed for the removal of carbon template. In this process, the Mn^{2+} ions were absorbed on the surface of carbon spheres, followed by the addition of ammonium persulfate (APS) and $AgNO_3$. They found that carbon spheres can be oxidized into CO_2 in APS and $AgNO_3$ solutions, which means that the carbon spheres as a reactive template can be removed during the reaction at room temperature.

(IV) Polystyrene (PS) spheres. The synthetic route of the PS spheres is quite simple, and furthermore, the particle sizes and surface functional groups of the PS spheres can be easily controlled. So, it is one of the most commonly used templates to synthesize metal oxide hollow nanostructures. The general procedure to synthesize metal oxide hollow nanostructures using PS spheres as a template involves two steps. First the metal salt precursor coats on the surface of the PS spheres by precipitation or directly reacting with the surface functional groups, and second the PS sphere template is calcined or dissolved to obtain the final hollow nanomaterials. Recently, using sulfonate groups ($-SO_3H$) functionalized PS hollow spheres as template, Ding et al. were able to prepare hierarchical NiO nanosheet hollow spheres [45]. The preparation process involves the absorption of Ni salt precursor on the surface of PS hollow spheres followed by the calcination which removes PS sphere template and finally the conversion of Ni precursor to NiO. Yang and co-workers have described an interesting approach to prepare inorganic double shelled hollow spheres via preferential adsorption of inorganic precursors into the sulfonated double shell layer of polystyrene (PS) templates [46]. As shown in Fig. 2A, a polystyrene hollow sphere containing a thin hydrophilic inner layer and transverse channels of PMMA–PMA was treated with sulfuric acid, and sulfonation took place in three locations: the exterior shell surface, the interior shell surface, and the transverse channels. This procedure created a hollow sphere that contained hydrophilic inner layer and outer layer, and channels of

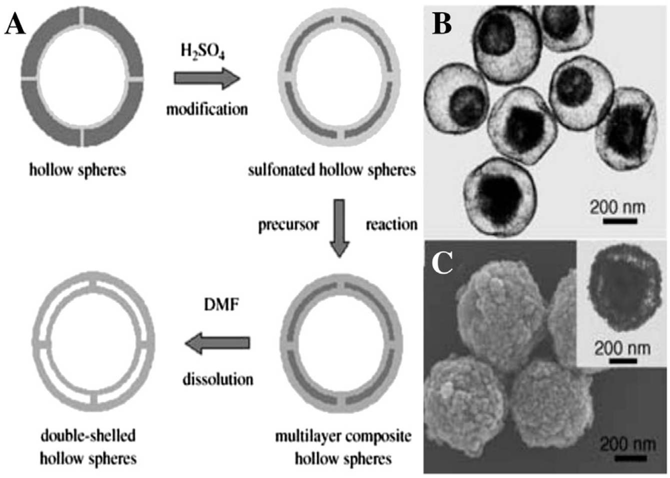

Fig. 2. A) Schematic illustration of the formation of double-shelled hollow spheres; B) TEM images of TiO_2 doubled hollow spheres and C) SEM images and TEM images (inset) of Fe_3O_4. Reproduced from [46]. Copyright 2005, Wiley-VCH.

sulfonated polystyrene gel. Metal salt precursors were absorbed by the outer layer and formed dense metal precursor layer which were also able to penetrate into the inner layer of the PS spheres via the created channels, and similarly formed a dense layer due to the existed functional groups of the inner layer. In the final process, the PS spheres were removed and the metal oxide double shelled hollow spheres were formed. Fig. 2B and C shows the TEM and SEM image of TiO_2 and Fe_3O_4 double shelled spheres templated by the as prepared PS spheres.

Electrodeposition method was often used to prepare hollow spheres by employing PS spheres as templates. Recently, Co_3O_4 hollow spheres with different morphologies have been prepared by Tu's group and reported in the literature [47–49]. It was observed that the morphological evolution of the synthesized hollow nanomaterials can be realized via adjusting the deposition parameters such as current density, deposition time and precursor concentration.

(V) Sacrificial templates. Sacrificial templates are a special class of hard templates to synthesize hollow metal oxide nanostructures. The main characteristic of sacrificial templates that different from the traditional hard templates is that they act as a precursor and involve in the synthetic process of the hollow nanomaterials. The sacrificial template is finally consumed partially or completely. Similar to the traditional hard templates, sacrificial template determines the final shape and cavity size of the resultant hollow materials. Fei et al. fabricated uniform MnO_2 nanospheres and nanoboxes by using $MnCO_3$ nanospheres and nanocubes as sacrificial templates [50]. The synthesis was performed by a three-step process. First, discrete spherical and cubic $MnCO_3$ precursors were prepared. Next, by changing the amounts of $KMnO_4$, the shells of the $MnCO_3$ precursors could be converted to MnO_2 with different shell thicknesses. Finally, the inner $MnCO_3$ cores could selectively be removed by HCl and hollow MnO_2 spheres and cubes were obtained.

Wang et al. developed a general sacrificial hard template method to prepare metal oxide hollow nanostructures based on controlled decomposition–dissolution (CDD) process of single metal-salt source [51]. The preparation process and their synthetic idea can be well understood in Fig. 3A. The fabrication process can be divided into several steps. In step a, partial thermal decomposition of metal salts (yellow) in air at an intermediate temperature leads to the formation of metal oxide outer layers (red) and leaves the cores unaffected (yellow); step b is dissolution of the residual metal salt core, producing hollow porous metal oxide shells; In the

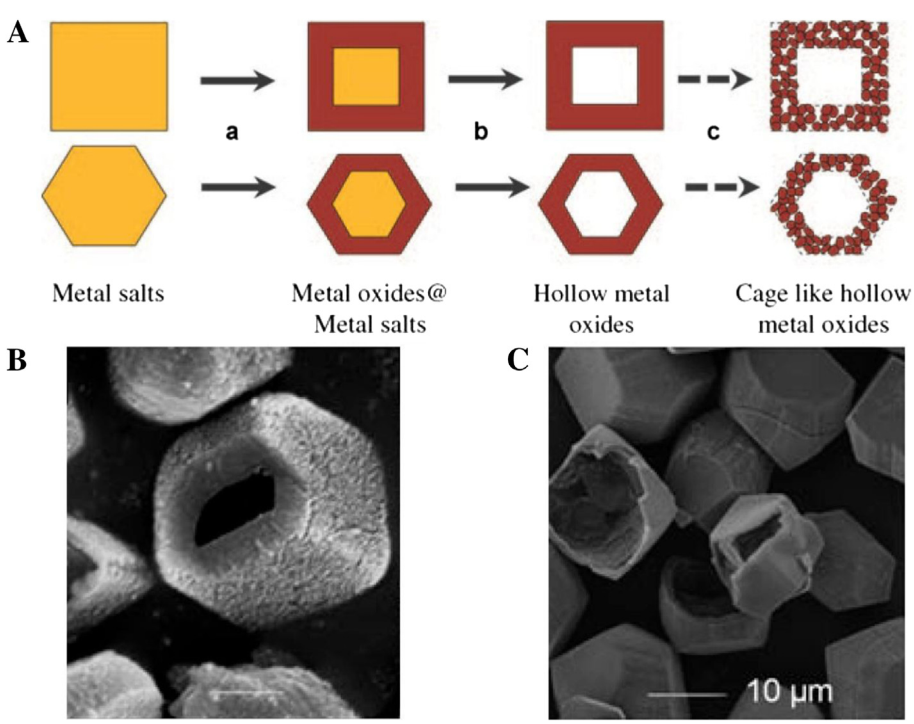

Fig. 3. A) Schematic illustration of the proposed controlled decomposition–dissolution method for the fabrication of nanoporous hollow structures; B) SEM images of MnO_2 nanoboxes and C) Fe_2O_3 hollow nanoparticles. Reproduced from [51]. Copyright 2009, Wiley-VCH.

final stage at step c, with further calcination, the prepared materials form cage-like hollow structures and further thermo-induced structural shrinkage occurs at higher temperatures. By using this method, Fe, Co, Ni, and Mn oxides hollow nanostructures had been successfully prepared [51]. Fig. 3B and C shows SEM images of MnO_2 nanoboxes and Fe_2O_3 hollow nanoparticles, respectively.

Except the sacrificial template method, the hard template method often involves the preparation of templates, coating of nanocrystals on the template surface, and finally removal of the template using calcination or etching. The advantages of the hard-template method can be summarized as follows: (i) it is a general tool to prepare hollow nanostructures with various morphologies; (ii) the diameter/hollow cavity of the products can be well controlled by the size of the templates; (iii) the products usually have uniform particle size and regular morphology. On the other hand, disadvantages of the hard-template method can be concluded as: (i) a series of post-processing is required to remove the template, which complicates the preparation process, and the post process may destroy or disorder the formed products to some extent; (ii) in this process, it is difficult to synthesize the product in large scale, (iii) nanomaterials produced by this process are usually not cost-effective. Moreover, the sacrificial template method is limited due to the insufficient availability of the raw materials.

3.1.2. Soft template methods

The soft template method to prepare metal oxide hollow nanostructures involves the formation of relatively flexible structures such as emulsion droplets, surfactants and gas bubble, etc. The growth of the target material first produces the shell and subsequently proceeds along the interfacial region during the removal of the template. Compared with hard template method, soft template-based methods hold appeal due to the easy removal of the templates compared with hard templates. However, due to the intrinsic shortcomings of soft templates such as thermodynamically unstable and structural unstable, it is hard to control the size, uniformity and microstructure of the inorganic hollow structures. Nevertheless, some infusive progresses have been made in recent years in some familiar anode materials such as Fe_2O_3, Cu_2O and Co_3O_4.

Lou's group reported α-Fe_2O_3 hollow spheres with well-defined hollow structures by a quasiemulsion-template method [20]. In their synthetic procedure, glycerol was first dispersed in water and formed oil-in-water quasiemulsion microdroplets, and then Fe precursor was assembled on the surface of the droplets. During the hydrothermal process, the Fe precursor was transformed to crystalline Fe_2O_3. Since the inner glycerol quasidroplet can be easily removed by solvent, the synthesized Fe_2O_3 shells possess good structural stability. Moreover, the synthesized Fe_2O_3 hollow spheres possess well-defined structures.

The self-assembly of surfactant molecules in aqueous solution leads to the formation of micelles and the close bilayers aggregate vesicles or dynamic nanostructures. These formed micelles and vesicles can be used as soft templates to synthesize hollow structures. Xu et al. developed a facile route to synthesize single- and multi-layer Cu_2O hollow spheres by using CTAB vesicles and multilamellar vesicles as soft templates [52]. In this work, authors presented that by simply controlling the concentration of CTAB (from 0.08 M to 0.15 M), single-, double-, triple-, and even quadruple-shelled Cu_2O hollow spheres with uniform particle size can be obtained as illustrated in Fig. 4A. Fig. 4B–E shows the TEM images of single-, double-, triple- and quadruple-shelled Cu_2O hollow spheres. With the similar synthetic idea, Wang et al. extended their work by successfully synthesizing single-, double- and triple-shelled Co_3O_4 hollow spheres with the help of PVP soft templates [12]. These spheres possess well mono-dispersed particles and uniform particle size. In addition, large-scale Co_3O_4 products can be obtained via this PVP-template method.

There are various other reports related with soft template method to prepare metal oxide hollow structures. Several examples are mentioned as follows. Li et al. demonstrated the fabrication of novel Fe_2O_3 hollow spheres by a facile hydrothermal treatment of the $K_4Fe(CN)_6$ and $(NH4)_2S_2O_8$ mixture in the presence of cetyltrimethyl ammonium bromide (CTAB) [53]; Mao et al. have synthesized hollow Fe_2O_3 spheres by a polyoxometalate-assisted hydrolysis process of Fe^{3+} under hydrothermal conditions [54]. Zeng et al. have synthesized hollow hematite spindles and microspheres using a hydrothermal method [55]. They speculated that the CO_2 bubbles released from urea could act as a soft template for the formation of such hollow structures. Wang et al. synthesized

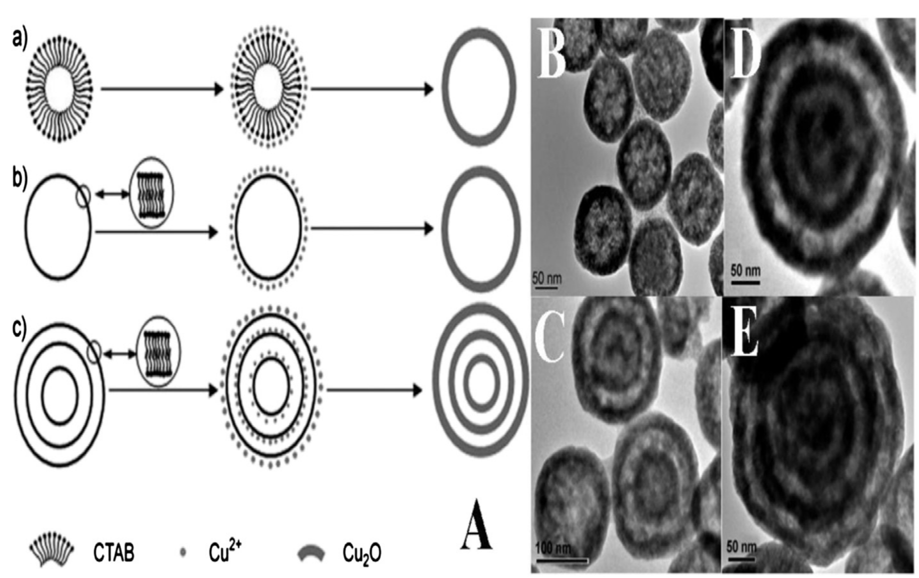

Fig. 4. A) Schematic illustration of the formation of different Cu_2O hollow structures with the assistance of CTAB template; B–E) TEM images of single-, double-, triple- and quadruple-shelled Cu_2O hollow spheres. Reproduced from [52]. Copyright 2007, Wiley-VCH.

SnO_2 nanotubes via a facile solution method with the assistance of PVP soft templates [56].

3.2. Template free method

Template method is an efficient, controllable, and conventional route to prepare hollow nanostructures, however, as mentioned in the above sections, the removal of the template suffers from the drawbacks of tedious procedures such as calcination and wet chemical etching, which results in disorder or destruction of the hollow-structures and this can even affect the chemical structure of the as-prepared products. Therefore, simpler methods for controllable preparation of hollow structures in a wide range of sizes would be more preferred. To date, a number of methods for the generation of hollow inorganic structures have been developed employing novel mechanisms, including the Kirkendall effect and the inside-out Ostwald ripening process. In this section, we will discuss the hollow structured metal oxide anodes synthesized by these two novel mechanisms.

3.2.1. Kirkendall effect

The Kirkendall effect, which originally explains how void space on zinc side is produced when a copper and a zinc metal are pressed against each other at an elevated temperature [57], has been developed as an useful tool for the synthesis of hollow structured materials. The essence of the Kirkendall effect based methods is to choose an appropriate diffusion couple, and during the synthesis, one component is either diffused through the interface or converted to the desired species with higher lattice density, thus leaving the original space void.

Typically, the formation mechanisms of a metal oxide hollow nano-structure can be summarized as follows. When a metal nanoparticle is exposed to oxygen (O) precursor under elevated temperatures, as the outward diffusion of metal cations is much faster than the inward diffusion of O anions, an inward flux of vacancies accompanies the outward metal cation flux to balance the diffusivity difference. When the vacancies reach a sufficient number, a larger hollow interior would emerge and thus, metal oxide hollow nano-structures are formed. Similarly, the mechanism is suitable for other metal compounds, such as metal sulfide, and selenide. For example, a series of cobalt compounds such as CoO, CoS_x, and CoSe were synthesized by Yin et al. [58]. Fig. 5 shows the morphology evolution of Co nanoparticles when exposed to O_2/Ar mixture and it can be found that Co nanocrystals were completely transformed to CoO hollow nanospheres due to the Kirkendall effect proposed by the authors.

Following their work, a number of metal oxide hollow nanostructures were synthesized based on Kirkendall effect. For example, one-dimensional (1D) chain-like arrays of hollow Fe_3O_4 spheres have been reported by simply aging magnetically pre-assembled Fe nanoparticles in aqueous solution at room temperature [59], and the hollow interior of the Fe_3O_4 spheres has a similar formation mechanism as proposed by Yin et al. [58]. Hollow Co_3O_4 nanowire arrays were prepared via a self-supported hydrothermal method. Authors proposed that the formation of hollow Co_3O_4 nanowire arrays is due to the synergy between axial screw dislocation and the Kirkendall effect [60]. Song et al. proposed a novel approach to synthesize porous NiO nanotubes with controllable interior voids based on an effective interplay between Kirkendall effect and volume change upon phase transformation [61]. Wu et al. synthesized SnO_2-carbon hybrid hollow spheres [62], and evidence indicated that the nanoscale Kirkendall effect plays a critical role in the transformation from Sn spheres to the hybrid hollow spheres. Via an alkylphosphonic acid assistant Kirkendall effect process, An et al. synthesized Fe and Mn oxide hollow nanostructures [63]. The etching of metal cations by alkylphosphonic acid on the surface of

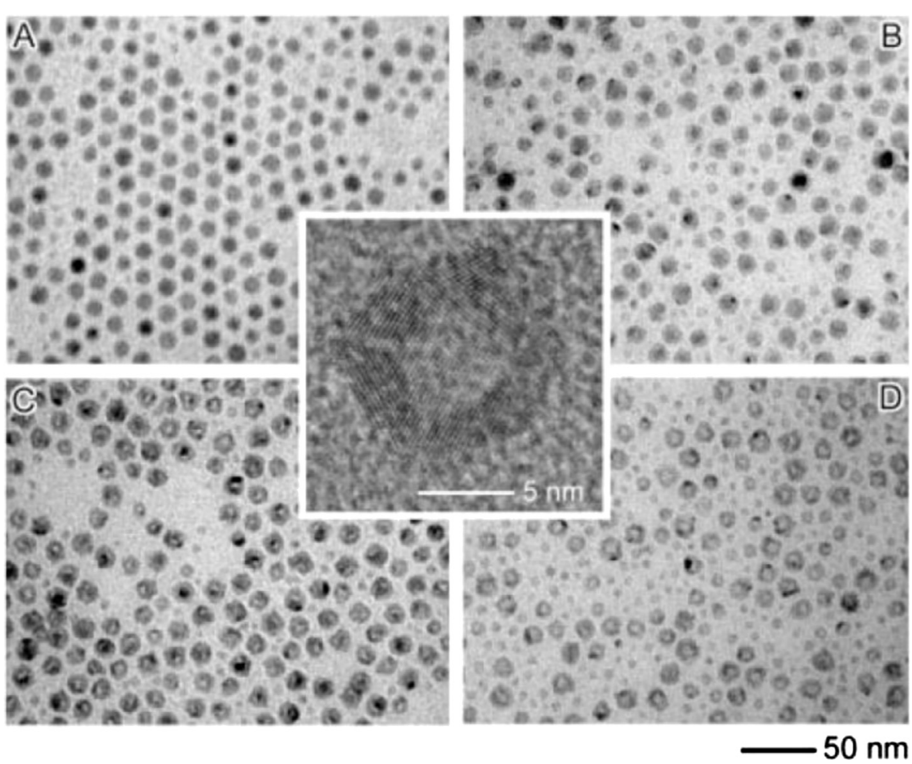

Fig. 5. Time-dependent morphology evolution of Co nanoparticles when exposed to O_2/Ar mixture at 455 K. (A) 0 min, (B) 30 min, (C) 80 min, (D) 210 min and the inset is the HRTEM image of a CoO hollow nanocrystal. Reproduced from [58]. Copyright 2004, Science.

metal oxide (Fe_2O_3, MnO) nanocrystals drives the outward diffusion of metal cations in the nanocrystals and results in the formation of void in the core. Based on the combination of the Kirkendall effect, volume loss, and gas release, Liu et al. developed a general top-down strategy to fabricate transition metal oxide hollow architectures [64], and they took CuO hollow structures as an example to illustrate their fabrication idea.

So far, a series of metal oxide hollow nanostructures have been prepared based on Kirkendall effect. No tedious fabrication and removal of template are needed in the fabrication processes. It is believed that the use of the Kirkendall effect allows a rational design of metal oxides hollow nanostructures, based on the proper choice of materials and different reaction properties.

3.2.2. Inside-out Ostwald ripening

In a high temperature solution reaction system, during Ostwald ripening process, large clusters or particles grow at the expense of small ones that eventually dissolve completely. The driving force, for both coalescence and ripening, is the lowering of the surface energy which is related to the surface area. The difference in solubility of clusters with different sizes and surface curvatures leads to the dissolution of small clusters and growth of larger ones. Thus, voids gradually form and grow in the cores of large aggregates owing to the persistent expense of the inner particles due to their higher solubility. Recently, the Ostwald ripening process is proposed as an important template free method to synthesize metal oxide hollow nanostructures.

Many metal oxide hollow nanostructures were synthesized based on the inside-out Ostwald ripening mechanism, such as SnO_2 [65,66], Fe_2O_3 [10,55,67,68], CoO [69,70], NiO [71], MnO_2 [72], CuO and Cu_2O [73,74]. Lou et al. synthesized SnO_2 hollow spheres via the inside-out Ostwald ripening process by a one-pot solvothermal method [65]. The particle size of the SnO_2 hollow spheres can be adjusted by changing the precursor concentration. Due to the larger surface energy of the inner particles, they have higher tendency to dissolve compared with the outer particles of the SnO_2 spheres. In addition, the primary particles in the outer surfaces are relatively easy to crystallize. Thus, the hollow SnO_2 spheres were formed. Recently, our group synthesized hollow SnO_2 spheres assembled by single crystalline nanoparticles [66]. The hollow spheres have well-dispersed spherical particles with an average diameter of 200 nm (Fig. 6A–D). The formation mechanism of Ostwald ripening process was confirmed by the time dependent experiment.

Chen et al. prepared porous hollow Fe_3O_4 beads with an average size of 700 nm via a solvothermal method [10]. The as-prepared beads were spherical in morphology and had good mono-dispersion. Via a series of time-dependent experiments, they carefully observed the morphology and constitution evolution of the products and proposed a four-step formation process of the porous hollow Fe_3O_4 beads. In the initial step, spindle-like Fe_2O_3 nanoparticles were formed under the solvothermal condition. In the following step, the Fe_2O_3 nanoparticles were reduced to Fe_3O_4 nanoparticles by ethylene glycol (EG). Next, under the combined effects of surfactants and water, well-defined Fe_3O_4 spheres were formed in 2 days. In the last step, Fe_3O_4 spheres evolved into porous and hollow Fe_3O_4 beads due to the Ostwald ripening process under the solvothermal condition.

In addition, metal oxide complex can be synthesized from the Ostwald-ripening-based self-templated method. Yu et al. prepared CuO/Cu_2O composite hollow microspheres using $Cu(CH_3COO)_2 \cdot H_2O$ as precursor via a hydrothermal method [74]. They found that the diameter from 0.5 to 5 μm of the microspheres could be adjusted via changing the precursor concentration (0.02–0.2 M), and the Cu_2O content from 20 to 80 wt.% in the CuO/Cu_2O composite could be controlled by changing the precursor concentration and the reaction time. A self-transformation process of the meta-stable aggregated particles accompanied by the localized Ostwald ripening was proposed to account for the formation of CuO/Cu_2O composite hollow microspheres.

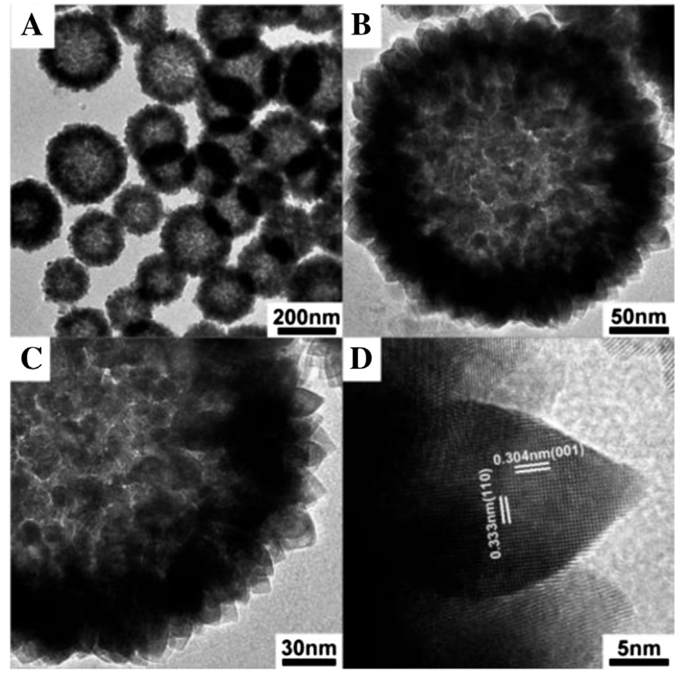

Fig. 6. TEM (A–C) and HRTEM (D) images of SnO_2 hollow nanospheres at different magnifications. Reproduced from [66]. Copyright 2012, The Royal Society of Chemistry.

Compared with hard/soft template based methods, Ostwald-ripening-based methods have obvious advantages in preparing metal oxide hollow nanostructures: i) having no problem resulting from template dissolution that exists in hard template method; ii) products with uniform particle size and morphology that cannot be easily obtained by soft template method. However, due to the deficiency of direct evidences, the exact formation mechanisms of metal oxides hollow strictures via Ostwald-ripening-based methods still need to be further studied.

4. Li storage properties of hollow metal oxide anode materials

4.1. SnO_2 hollow structures

Since it has been discovered as an important potential anode material for LIBs with high capacity, SnO_2 has attracted wide attention [75]. However, as mentioned in Section 2.3, the biggest problem that hinders the practical use of the material is the fast capacity fading upon cycling. Thus, the hollow structures have attracted particular attention because of their improvable electrochemical performances, especially cycling performance.

Lou et al. reported a one-pot solvothermal synthesized SnO_2 hollow nanospheres [65]. As anode material for LIBs, the SnO_2 hollow nanospheres showed high initial reversible charge capacity of 1140 mAh g^{-1} and improved cycling performance. The ultrahigh lithium storage capacity can be attributed to the nanopores in the shells and interior cavities of hollow nanospheres, which can store some extra Li ions. After 30 cycles, the SnO_2 hollow spheres still exhibited a high reversible charge capacity close to the theoretical value, with 70% of the initial charge capacity remaining. Later on, the same group prepared SnO_2 hollow nanospheres by using mesoporous silica template [28]. The SnO_2 hollow nanospheres

showed improved cycling performance compared with SnO_2 solid spheres and nanoparticles. The SnO_2 hollow nanospheres exhibited a reversible charge capacity more than 700 mAh g^{-1}, while the values were less than 600 mAh g^{-1} for the SnO_2 solid spheres and nanoparticles. At last they suggested that the performance could be further improved by coating hollow SnO_2 spheres with a thin layer of carbon materials [76,77]. In fact, better cycling performance can also be obtained by tailoring the hollow structure of SnO_2 [78].

The none-spherical SnO_2 hollow structures also showed obvious advantages as anode materials for LIBs. For example, Wang et al. prepared SnO_2 nanotubes by using AAO as template [31]. In Fig. 7, curves a and b show the initial charge/discharge capacities and cycling performances of the SnO_2 nanotubes and nanoparticles, respectively. The SnO_2 nanotubes exhibited an initial capacity of 940 mAh g^{-1}, and after 80 cycles, the value can be retained as high as 525 mAh g^{-1}, which corresponds to 55.8% of the initial specific capacity. In contrast, the SnO_2 nanoparticles showed an initial specific capacity of 676 mAh g^{-1}, and this value dropped to 65 mAh g^{-1} after 80 cycles, corresponding to only 9.6% of the initial value. More recently, Lou's group prepared SnO_2 nanoboxes using Cu_2O nanocubes as sacrificial template [34]. When tested as anode materials for LIBs, the as-prepared material exhibited satisfying electrochemical performances. The initial discharge and charge capacities of the annealed sample are found to be 2242 and 1041 mAh g^{-1}, respectively. They suggested that the ultra-high initial capacities might be associated with the unique structure of the hollow nanoboxes with nanoporous shells. After 40 cycles, the capacity of the annealed sample can still remain above 570 mAh g^{-1}. All these results clearly reveal the suitability of SnO_2 hollow materials for LIBs applications.

4.2. Fe, Co and Ni oxides hollow structures

It is reported that 3D transition-metal oxides such as nickel oxides, cobalt oxides, and iron oxides exhibit reversible capacities

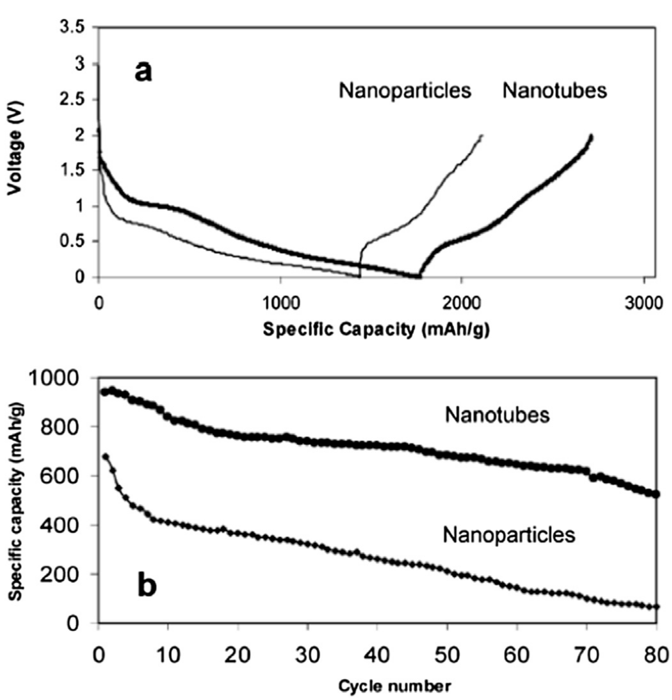

Fig. 7. a) The first cycle charge–discharge curves of SnO_2 nanotube and nanoparticle electrodes. b) Cycling performance of SnO_2 nanotube electrodes and SnO_2 nanoparticle electrodes. Reproduced from [31]. Copyright 2005, American Chemical Society.

about three times larger than those of graphite [4,79]. Similar to the SnO_2 anode, the notorious problems of 3D transition-metal oxides as anode materials are the poor cycling performance. Recently, the enhanced electrochemical performance of iron, cobalt and nickel oxides has been reported through the fabrication of hollow nanostructures [20,80,81].

Lou's group prepared α-Fe_2O_3 hollow spheres using a quasiemulsion-templated method [20]. The as-prepared Fe_2O_3 hollow spheres show an apparent advantage compared with Fe_2O_3 microparticles as LIB anode materials. The Fe_2O_3 hollow spheres gave an initial discharge capacity of 1219 mAh g^{-1} accompanied with the charge capacity of 877 mAh g^{-1}. From the second cycle on, the capacity keeps stable at $\sim$750 mAh g^{-1}. Even after 100 cycles, a reversible capacity as high as 710 mAh g^{-1} can still be retained. In contrast, the Fe_2O_3 microparticles show a much lower initial discharge capacity and the capacity drops quickly to 340 mAh g^{-1} at the end of the test.

Wang et al. synthesized single, double and triple shelled Co_3O_4 hollow spheres using PVP as soft templates [12]. As shown in Fig. 8A, the first discharge capacities of the samples S-Co (single shelled Co_3O_4), D-Co (double shelled Co_3O_4), and T-Co (triple shelled Co_3O_4) were 1199.3, 1013.1 and 1528.9 mAh g^{-1}, respectively, all of which are higher than their theoretical values (890 mAh g^{-1}). When tested at 0.2C, the capacities of S-Co, D-Co, and T-Co still remained as high as 680, 866, and 611 mAh g^{-1}, respectively, after 50 cycles. In contrast, the C-Co (commercial Co_3O_4) showed an initial capacity of 1029 mAh g^{-1}, but only had a reversible capacity of 134 mAh g^{-1} left after 20 cycles (Fig. 8B). The hollow nanostructured Co_3O_4 showed superior electrochemical performance compared with the commercial product. The above result also implies the D-Co exhibited best cycling performance and the authors suggested that the void space in the D-Co was appropriate, which not only correctly accommodated the volume after expansion, leading to a larger contact surface with the electrolyte, but also kept the structure stable during cycling. In addition, the D-Co exhibited good high-rate performance, as shown in Fig. 8C. Even at a high current rate of 2C, this material can still deliver a capacity of 500.8 mAh g^{-1}.

The NiO hollow microspheres prepared by Huang et al. showed much better cycling performance compared with the irregular NiO particles and solid spheres [80]. The first discharge/charge capacities of the NiO hollow microspheres were 1100 and 620 mAh g^{-1}, respectively. Until the 45th cycle, the discharge and charge capacities were still as high as 560 and 490 mAh g^{-1}, respectively. The reversible capacity remained up to 80% of the initial capacity (charge capacity).

The tubular Fe and Co oxide hollow structures exhibited satisfying cycling performance when used as anode materials for LIBs. For example, most recently, Kang et al. prepared Fe_2O_3 nanotubes (FNT) mainly consisting of γ-Fe_2O_3 phase using microporous organic nanotubes as template [81]. As shown in Fig. 9a and b, the FNT showed a reversible discharge of 950 mAh g^{-1} in the second cycle. After 30 cycles there were still 929 mAh g^{-1} left, and the capacity retention reached up to 97.8%. The FNT exhibited high coulombic efficiency. The initial coulombic efficiency was 71% and maintained a high value above 97% after the fourth cycle. The capacity loss was only 26% between the first and second discharge cycle. The excellent performance was comparable with the best reported value of the non-composite hollow α-Fe_2O_3 materials. In comparison, the commercial γ-Fe_2O_3 nanoparticles showed a rapid capacity loss during cycling. What's more, the FNT also showed excellent high-rate performance, as can be seen from Fig. 9c. Even at the current density of 0.5 and 1 A g^{-1}, the discharge capacities of 918 mAh g^{-1} and 882 mAh g^{-1}, respectively, can be obtained. The Co_3O_4 nanotubes prepared by Lou et al. showed perfect

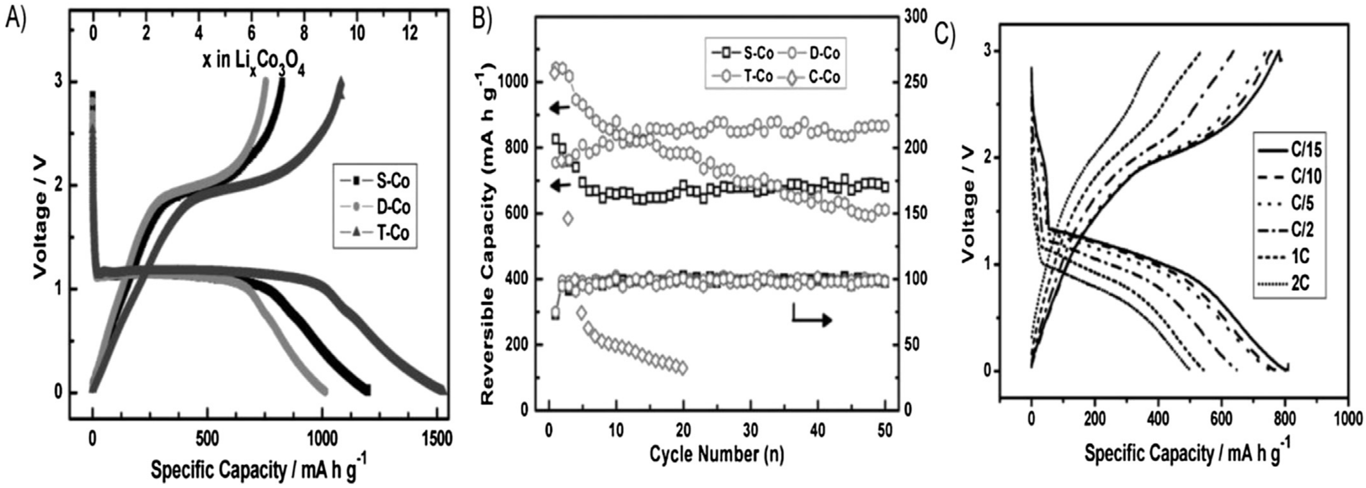

Fig. 8. A) First cycle discharge–charge profiles of S-Co, D-Co, and T-Co. B) Cyclability and coulombic efficiency of the three as-prepared samples and commercial Co_3O_4 products (C-Co). C) Charge–discharge profiles of D-Co at different current densities. Reproduced from [12]. Copyright 2010, Wiley-VCH.

electrochemical performance [82]. Despite large initial capacity loss, a high charge capacity of 950 mAh g^{-1} was still attained in the first cycle. Even after 30 cycles, the charge capacity of 918 mAh g^{-1} was maintained, corresponding to a fading rate of only 0.1% per cycle. Although the capacity faded faster after 30 cycles, the capacity was still comparable to the theoretical capacity of graphite after 80 cycles.

4.3. Cu oxide hollow structures

Although the electrochemical performance of CuO or Cu_2O hollow structures as LIBs' anode materials have not been widely investigated, their advantages compared with the bulk or irregular CuO or Cu_2O anodes have been already confirmed by some literature [83–86]. For example, although the CuO hollow nanospheres prepared by Kong et al. did not show satisfying electrochemical performance, they displayed better cycling performance than CuO nanoparticles [85]. Wang et al. prepared Dandelion-like CuO hollow microspheres via a hydrothermal process [86]. As LIB anode materials, the CuO hollow microspheres showed an initial discharge capacity of 1274 mAh g^{-1} and a high reversible (charge) capacity up to 750 mAh g^{-1}. In addition, the materials showed a negligible capacity fading even after 50 cycles at the current rate of 0.2C. Even at 2C rate, the material exhibited a high reversible capacity of 490 mAh g^{-1} and furthers a good cycling performance after 35 cycles.

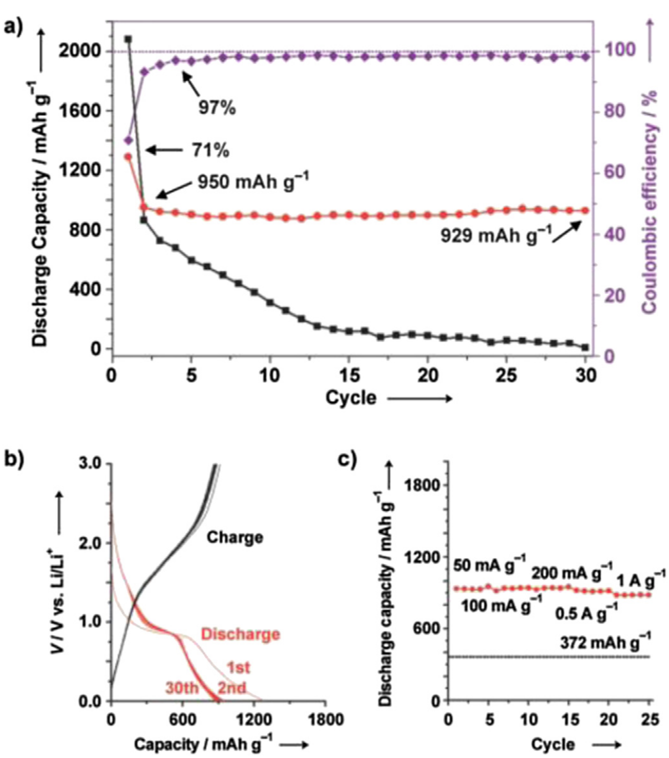

Fig. 9. a) Discharge capacities of the Fe_2O_3 nanotubes (●), commercial γ-Fe_2O_3 nanoparticles (■) and coulombic efficiencies of Fe_2O_3 nanotubes (◆) upon cycling numbers; b) charge–discharge curves and c) rate performance of the Fe_2O_3 nanotubes. Reproduced from [81]. Copyright 2012, Wiley-VCH.

4.4. Mn oxide hollow structures

In the past decade, MnO_2 has been investigated as an effective anode material for LIBs because of its low cost, low toxicity and high capacity. The electrochemical performance of the material has been significantly improved by the fabrication of its hollow nanostructures [87,88]. Zhao et al. prepared γ-MnO_2 hollow microspheres by using a hydrothermal method [87]. As LIBs anode materials, the hollow microspheres displayed an initial reversible capacity of 1071.1 mAh g^{-1}. The initial coulombic efficiency reached up to 83.1% after 20 cycles, and the discharge capacity for the hollow microsphere still maintained at 602.1 mAh g^{-1}. Li et al. prepared α-MnO_2 hollow urchins by a low-temperature mild reduction route [88]. The as-prepared α-MnO_2 hollow urchins exhibited much better electrochemical performance than the solid urchins and dispersed nanorods. For α-MnO_2 hollow urchins, a high capacity of 746.0 mAh g^{-1} was obtained in the first discharge process, while the discharge capacities of solid urchins and dispersed nanorods were 384.3 and 528.1 mAh g^{-1}, respectively. At a current density of 270 mA g^{-1}, the capacity still remained as high as 481 mAh g^{-1} after 40 cycles, indicating the excellent cycling performance of the hollow urchins.

5. Conclusion and future prospects

In conclusion, we have summarized the recent progress in various synthesis techniques of metal oxide (SnO_2, Fe_2O_3, CoO, Co_3O_4, NiO, CuO and MnO_2 etc.) hollow materials and their efficient utilization as anode materials for the fabrication of LIBs. It was

observed that by applying various synthetic technologies, a variety of morphologies of high quality metal oxide hollow nano/microstructures can be obtained. For example, metal oxide hollow spheres, nanotubes and nanoboxes with monodisperse state, uniform shape, controlled size and shell thickness have been successfully prepared by using template/and or template-free methods. When applied as anode materials for LIBs, the metal oxide hollow nano/microstructures display improved electrochemical performances compared with the bulk or nanoparticle materials. Specifically, they exhibit higher capacity, better cycling performance and rate capacities. It is concluded that there are three obvious advantages of hollow nanostructures of metal oxides compared with their corresponding bulk materials or nanoparticles as anode materials for LIBs: i) higher discharge/charge capacities; ii) better cycle performance and iii) high rate capacities. The improved electrochemical performances of the hollow nanostructures originate from the following factors: i) the hollow structures can provide large electrode/electrolyte contact area and store Li ions in the surface and nanopores beside the grain lattice and interface storage, both of which lead to higher capacity; ii) the thin shells afford short diffusion lengths for both lithium ion and electron transport, thus greatly improves the materials' rate capacities; iii) the hollow and mesoporous structures can easily suppress the large volume change during charging/discharging processes, which will retain better stability and cyclability.

However, challenges still exist both in material synthesis and electrochemical performances. For the synthesis, so far, no single method exists that can produce all kinds of metal oxide hollow nano/microstructures with high quality. Furthermore, almost none of the known methods are industrially available to produce hollow nano/microstructures materials. In addition, most of the known methods are either time-consuming or costly. As a result, there is still a long way to realize the commercialization of the hollow structured metal oxide anodes. Therefore, efficient synthetic methods are urgently needed to be developed in order to meet the practical use of these materials as anodes for LIBs. As for the Li storage property, although the cycling performance and high rate property of the hollow metal oxide structures are indeed improved compared with the bulk or particle materials, further modification is still needed in order to satisfy the practical demands. The main problem that causes the capacity decrease of metal oxide hollow structures is their structural instability during cycling, and therefore, hybriding them with some flexible materials such as graphene is an ideal rout to solve this problem [89]; For electrode materials, carbon coating and/or hybriding them with other efficient conductive materials have already been demonstrated as an effective way to further improve their high rate performance as reported in literature [90–93], the method is equally applicable to hollow metal oxide anodes [90,91]. Another problem that commonly exists in the metal oxide anodes, especially for the alloying model metal anodes, is the large irreversible capacities in the initial cycle. Until now, few methods reported can thoroughly deal with this problem. In addition, although the relationship between the electrochemical performances and the morphologies has been investigated for years, some electrochemical properties, such as the ultra-high initial capacity of the hollow structures, still puzzle people. Deep understanding of the relationship between the morphologies of hollow metal oxide nanostructures and their applications as anode material for LIBs is needed and should be explored extensively.

Acknowledgments

This work was financially supported by National Basic Research Program of China (Nos. 2011CB935704, 2013CB934004, 2010CB934700), the National Natural Science Foundation of China (Nos. 11079002, 20111102130006), Research Fund of Ministry of Education of China (No. 20110002130007). Ahmad Umar would like to acknowledge the Ministry of Higher Education, Kingdom of Saudi Arabia for granting a Promising Centre for Sensors and Electronic Devices (PCSED) dated 24/3/1432 H, 27/02/2011 to Najran University.

References

[1] A.K. Shukla, T.P. Kumar, Curr. Sci. 94 (2008) 314.
[2] M. Winter, J.O. Besenhard, M.E. Spahr, P. Novak, Adv. Mater. 10 (1998) 725.
[3] A. Courtney, J.R. Dahn, J. Electrochem. Soc. 144 (1997) 2045.
[4] P. Poizot, S. Laruelle, S. Grugeon, L. Dupont, J.M. Tarascon, Nature 496 (2000) 407.
[5] C.M. Julien, Mater. Sci. Eng. 40 (2003) 47.
[6] J. Cabana, L. Monconduit, D. Larcher, M. Rosa Palacín, Adv. Mater. 22 (2010) 170.
[7] K. Zhong, X. Xia, B. Zhang, H. Li, Z. Wang, L. Chen, J. Power Sources 195 (2010) 3300.
[8] Y. Li, X. Lv, J. Lu, J. Li, J. Phys. Chem. C 114 (2010) 21770.
[9] X. Zhu, Y. Zhu, S. Murali, M.D. Stoller, R.S. Ruoff, ACS Nano 5 (2011) 3333.
[10] Y. Chen, H. Xie, L. Liu, J. Xu, J. Mater. Chem. 22 (2012) 5006.
[11] C.H. Chen, B.J. Hwang, J.S. Do, J.H. Weng, M. Venkateswarlu, M.Y. Cheng, R. Santhanam, K. Ragavendran, J.F. Lee, J.M. Chen, D.G. Liu, Electrochem. Commun. 12 (2010) 496.
[12] X. Wang, X.L. Wu, Y.G. Guo, Y.T. Zhong, X.Q. Cao, Y. Ma, J.N. Yao, Adv. Funct. Mater. 20 (2010) 1680.
[13] X.P. Gao, J.L. Bao, G.L. Pan, H.Y. Zhu, P.X. Huang, F. Wu, D.Y. Song, J. Phys. Chem. B 108 (2004) 5547.
[14] J. Liu, W. Li, A. Manthiram, Chem. Commun. 46 (2010) 1437.
[15] Z.H. Wen, Q. Wang, Q. Zhang, J.H. Li, Adv. Funct. Mater. 17 (2007) 2772.
[16] D. Chen, L. Tang, J. Li, Chem. Soc. Rev. 39 (2010) 3157.
[17] J. Liang, W. Wei, D. Zhong, Q. Yang, L. Li, L. Guo, ACS Appl. Mater. Interfaces 4 (2012) 454.
[18] S.L. Candelaria, Y. Shao, W. Zhou, X. Li, J. Xiao, J. Zhang, J. Zhang, Y. Wang, J. Liu, J. Li, G. Cao, Nano Energy 1 (2012) 195.
[19] Q.G. Shao, W.M. Chen, Z.H. Wang, L. Qie, L.X. Yuan, W.X. Zhang, X.L. Hua, Y.H. Huang, Electrochem. Commun. 13 (2011) 1431.
[20] B. Wang, J.S. Chen, H.B. Wu, Z.Y. Wang, X.W. Lou, J. Am. Chem. Soc. 133 (2011) 17146.
[21] Y.M. Li, J.H. Li, J. Phys. Chem. C 112 (2008) 14216.
[22] H. Wang, Y. Wu, Y. Bai, W. Zhou, Y. An, J. Li, L. Guo, J. Mater. Chem. 21 (2011) 10189.
[23] Y.G. Li, B. Tan, Y.Y. Wu, Nano Lett. 8 (2008) 265.
[24] Y.G. Li, B. Tan, Y.Y. Wu, J. Am. Chem. Soc. 128 (2006) 14258.
[25] Y. Sun, X.Y. Feng, C.H. Chen, J. Power Sources 196 (2011) 784.
[26] H.C. Liu, S.K. Yen, J. Power Sources 166 (2007) 478.
[27] Y. Wu, Z. Wen, J. Li, Small 8 (2012) 858.
[28] S. Ding, J.S. Chen, G. Qi, X. Duan, Z. Wang, E.P. Giannelis, L.A. Archer, X.W. Lou, J. Am. Chem. Soc. 133 (2011) 21.
[29] X.W. Lou, C. Yuan, L.A. Archer, Adv. Mater. 19 (2007) 3328.
[30] T.A. Crowley, K.J. Ziegler, D.M. Lyons, D. Erts, H. Olin, M.A. Morris, J.D. Holmes, Chem. Mater. 15 (2003) 3518.
[31] Y. Wang, J.Y. Lee, H.C. Zeng, Chem. Mater. 17 (2005) 3899.
[32] G. Malandrino, S.T. Finocchiaro, R.L. Nigro, C. Bongiorno, C. Spinella, I.L. Fragala, Chem. Mater. 16 (2004) 5559.
[33] A.L.M. Reddy, M.M. Shaijumon, S.R. Gowda, P.M. Ajayan, Nano Lett. 9 (2009) 1002.
[34] Z. Wang, D. Luan, F.Y.C. Boey, X.W. Lou, J. Am. Chem. Soc. 133 (2011) 4738.
[35] Z. Wang, D. Luan, C.M. Li, F. Su, S. Madhavi, F.Y.C. Boey, X.W. Lou, J. Am. Chem. Soc. 132 (2010) 16271.
[36] D.F. Zhang, H. Zhang, Y. Shang, L. Guo, Cryst. Growth Des. 11 (2011) 3748.
[37] F. Hong, S. Sun, H. You, S. Yang, J. Fang, S. Guo, Z. Yang, B. Ding, X. Song, Cryst. Growth Des. 11 (2011) 3694.
[38] (a) A. Dong, N. Ren, Y. Tang, Y. Wang, Y. Zhang, W. Hua, Z. Gao, J. Am. Chem. Soc. 125 (2003) 4976;
(b) Z. Yang, Y. Xia, Adv. Mater. 16 (2004) 727;
(c) R. Mokaya, Adv. Mater. 16 (2004) 727.
[39] R. Yuan, X. Fu, X. Wang, P. Liu, L. Wu, Y. Xu, X. Wang, Z. Wang, Chem. Mater. 18 (2006) 4700.
[40] J.H. Bang, K.S. Suslick, J. Am. Chem. Soc. 129 (2007) 2242.
[41] D. Jagadeesan, U. Mansoori, P. Mandal, A. Sundaresan, M. Eswaramoorthy, Angew. Chem. Int. Ed. 120 (2008) 7799.
[42] H.S. Qian, G.F. Lin, Y.X. Zhang, P. Gunawan, R. Xu, Nanotechnology (2007) 18.
[43] L.S. Zhang, L.Y. Jiang, C.Q. Chen, W. Li, W.G. Song, Y.G. Guo, Chem. Mater. 22 (2010) 414.
[44] N. Wang, Y. Gao, J. Gong, X. Ma, X. Zhang, Y. Guo, L. Qu, Eur. J. Inorg. Chem. (2008) 3827.
[45] S. Ding, T. Zhu, J.S. Chen, Z. Wang, C. Yuan, X.W. Lou, J. Mater. Chem. 21 (2011) 6602.
[46] M. Yang, J. Ma, C.L. Zhang, Z.Z. Yang, Y.F. Lu, Angew. Chem. Int. Ed. 44 (2005) 6727.

[47] X.H. Xia, J.P. Tu, J.Y. Xiang, X.H. Huang, X.L. Wang, X.B. Zhao, J. Power Sources 195 (2010) 2014.
[48] X.H. Xia, J.P. Tu, X.L. Wang, C.D. Gu, X.B. Zhao, Chem. Commun. 47 (2011) 5786.
[49] X.H. Xia, J.P. Tu, J. Zhang, J.Y. Xiang, X.L. Wang, X.B. Zhao, ACS Appl. Mater. Interfaces 2 (2010) 186.
[50] J. Fei, Y. Cui, X. Yan, W. Qi, Y. Yang, K. Wang, Q. He, J. Li, Adv. Mater. 20 (2008) 452.
[51] L. Wang, F. Tang, K. Ozawa, Z.G. Chen, A. Mukherj, Y. Zhu, Jin Zou, H.M. Cheng, G.Q. Lu, Angew. Chem. Int. Ed. 48 (2009) 7048.
[52] H. Xu, W. Wang, Angew. Chem. Int. Ed. 46 (2007) 1489.
[53] L.L. Li, Y. Chu, Y. Liu, J. Phys. Chem. C 111 (2007) 2123.
[54] B.D. Mao, Z.H. Kang, E.B. Wang, C.G. Tian, Z.M. Zhang, C.L. Wang, Y.L. Song, M.Y. Li, J. Solid State Chem. 180 (2007) 489.
[55] S.Y. Zeng, K.B. Tang, T.W. Li, Z.H. Liang, D. Wang, Y.K. Wang, W.W. Zhou, J. Phys. Chem. C 111 (2007) 10217.
[56] N. Wang, X. Cao, L. Guo, J. Phys. Chem. C 112 (2008) 12616.
[57] A.D. Smigelskas, E.O. Kirkendall, Trans. AIME 171 (1947) 130.
[58] Y. Yin, R.M. Rioux, C.K. Erdonmez, S. Hughes, G.A. Somorjai, A.P. Alivisatos, Science 304 (2004) 711.
[59] J. Huang, W. Chen, W. Zhao, Y. Li, X. Li, C. Chen, J. Phys. Chem. C 113 (2009) 12067.
[60] X. Xia, J. Tu, Y. Mai, X. Wang, C. Gu, X. Zhao, J. Mater. Chem. 21 (2011) 9319.
[61] X. Song, L. Gao, S. Mathur, J. Phys. Chem. C 115 (2011) 21730.
[62] P. Wu, N. Du, H. Zhang, C. Zhai, D. Yang, ACS Appl. Mater. Interfaces 3 (2011) 1946.
[63] K. An, S.G. Kwon, M. Park, H.B. Na, S. Baik, J.H. Yu, D. Kim, J.S. Son, Y.W. Kim, I.C. Song, W.K. Moon, H.M. Park, T. Hyeon, Nano Lett. 8 (2008) 4252.
[64] J. Liu, D. Xue, Adv. Mater. 20 (2008) 2622.
[65] X.W. Lou, Y. Wang, C. Yuan, J.Y. Lee, L.A. Archer, Adv. Mater. 18 (2006) 2325.
[66] H. Wang, B. Li, J. Gao, M. Tang, H. Feng, J. Li, L. Guo, CrystEngComm 14 (2012) 5177.
[67] H.J. Song, X.H. Jia, H. Qi, X.F. Yang, H. Tang, C.Y. Min, J. Mater. Chem. 22 (2012) 3508.
[68] D. Du, M. Cao, J. Phys. Chem. C 112 (2008) 10754.
[69] G. Sun, X. Zhang, M. Cao, B. Li, C. Hu, J. Phys. Chem. C 113 (2009) 6948.
[70] R. Qiao, X. Li Zhang, R. Qiu, J.C. Kim, Y.S. Kang, Chem. Eur. J. 15 (2009) 1886.
[71] Y. Wang, Q. Zhu, H. Zhang, Chem. Commun. (2005) 5231.
[72] M. Xu, L. Kong, W. Zhou, H. Li, J. Phys. Chem. C 111 (2007) 19141.
[73] M. Yang, Y. Zhang, G. Pang, S. Feng, Eur. J. Inorg. Chem. (2007) 3841.
[74] H. Yu, J. Yu, S. Liu, S. Mann, Chem. Mater. 19 (2007) 4327.
[75] Y. Idota, T. Kubota, A. Matsufuji, Y. Maekawa, T. Miyasaka, Science 276 (1997) 1395.
[76] Y. Wang, F. Su, J.Y. Lee, X.S. Zhao, Chem. Mater. 18 (2006) 1347.
[77] Y. Wang, J.Y. Lee, J. Power Sources 144 (2005) 220.
[78] X.W. Lou, D. Da, J.Y. Lee, L.A. Archer, Chem. Mater. 20 (2008) 6562.
[79] D. Larcher, D. Bonnin, R. Cortes, I. Rivals, L. Personnaz, J.M. Tarascon, J. Electrochem. Soc. 150 (2003) A1643.
[80] X.H. Huang, J.P. Tu, C.Q. Zhang, F. Zhou, Electrochim. Acta 55 (2010) 8981.
[81] N. Kang, J.H. Park, J. Choi, J. Jin, J. Chun, I.G. Jung, J. Jeong, J.G. Park, S.M. Lee, H.J. Kim, S.U. Son, Angew. Chem. Int. Ed. 124 (2012) 1.
[82] X.W. Lou, D. Deng, J.Y. Lee, J. Feng, L.A. Archer, Adv. Mater. 20 (2008) 258.
[83] S. Gao, S. Yang, J. Shu, S. Zhang, Z. Li, K. Jiang, J. Phys. Chem. C 112 (2008) 19324.
[84] Y. Hu, X. Huang, K. Wang, J. Liu, J. Jiang, R. Ding, X. Ji, X. Li, J. Solid State Chem. 183 (2010) 662.
[85] M. Kong, W. Zhang, Z. Yang, S. Weng, Z. Chen, Appl. Surf. Sci. 258 (2011) 1317.
[86] S.Q. Wang, J.Y. Zhang, C.H. Chen, Scr. Mater. 57 (2007) 337.
[87] J. Zhao, Z. Tao, J. Liang, J. Chen, Cryst. Growth Des. 8 (2008) 2799.
[88] B. Li, G. Rong, Y. Xie, L. Huang, C. Feng, Inorg. Chem. 45 (2006) 6404.
[89] X. Zhou, Y.X. Yin, L. Wan, Y.G. Guo, J. Mater. Chem. 22 (2012) 17456.
[90] Y. Zhong, X. Wang, K. Jiang, J.Y. Zheng, Y. Guo, Y. Ma, J. Yao, J. Mater. Chem. 21 (2011) 17998.
[91] W.M. Zhang, J.S. Hu, Y.G. Guo, S.F. Zheng, L.S. Zhong, W.G. Song, L.J. Wan, Adv. Mater. 20 (2008) 1160.
[92] Y. Wu, Z. Wen, H. Feng, J.H. Li, Eur. J. Chem. (2013), http://dx.doi.org/10.1002/chem.201203535.
[93] Z.H. Wen, J.H. Li, J. Mater. Chem. 19 (2009) 8707.